

# SPS processing of bismuth-layer structured ferroelectric ceramics yielding highly textured microstructures

Jing Liu<sup>a</sup>, Zhijian Shen<sup>a,\*</sup>, Mats Nygren<sup>a</sup>, Yanmei Kan<sup>b</sup>, Peiling Wang<sup>b</sup>

<sup>a</sup> Department of Inorganic Chemistry, Arrhenius Laboratory, Stockholm University, SE-10691 Stockholm, Sweden

<sup>b</sup> Shanghai Institute of Ceramics, Chinese Academy of Science, 1295 Dingxi Road, Shanghai 200050, PR China

Received 18 May 2005; received in revised form 12 August 2005; accepted 16 August 2005

Available online 18 November 2005

## Abstract

The spark plasma sintering (SPS) behaviour of nano-sized  $\text{Bi}_4\text{Ti}_3\text{O}_{12}$  (BIT) and micron-sized  $\text{CaBi}_2\text{Nb}_2\text{O}_9$  (CBNO) powders is described. The densification process of both powders is very rapid, i.e. the densification occurs within a very narrow time interval (2–3 min using a heating rate of  $100^\circ\text{C min}^{-1}$  and a pressure of 50 MPa). The BIT powder exhibits a lower densification onset temperature ( $\sim 650^\circ\text{C}$ ) and higher maximum shrinkage rate ( $8.9 \times 10^{-3} \text{ s}^{-1}$  at  $780^\circ\text{C}$ ) than that of the CBNO powder ( $\sim 825^\circ\text{C}$  and  $4.5 \times 10^{-3} \text{ s}^{-1}$  at  $950^\circ\text{C}$ ). Isothermal compaction studies revealed that fully dense nano-sized BIT compacts could be obtained within the temperature region  $750^\circ\text{C} < T_{\text{iso}} < 850^\circ\text{C}$  while for  $T_{\text{iso}} > 850^\circ\text{C}$  compacts containing elongated platelet grains are formed. A new preparation route to produce highly textured compacts is described in detail. Appropriate pre-forms are prepared by spark plasma sintering (SPS) and these fully dense compacts are subject to superplastic deformation in the SPS unit to achieve a total compressive strain of  $\sim 60\%$ . This strain was achieved within a period of 1.5 min and with a maximum strain rates of  $1.1 \times 10^{-2} \text{ s}^{-1}$  achieved at  $\sim 840^\circ\text{C}$  and  $1.3 \times 10^{-2} \text{ s}^{-1}$  at  $1020^\circ\text{C}$  for the BIT and CBNO compacts, respectively. The X-ray studies showed that the Lotgering orientation factors of grains in the deformed BIT and CBNO compacts are 99% and 70%. The formation of highly textured compacts is suggested to be governed by a superplastic deformation-induced directional dynamic ripening mechanism.

© 2005 Elsevier Ltd. All rights reserved.

**Keywords:** Sintering; Grain growth; SPS;  $\text{Bi}_4\text{Ti}_3\text{O}_{12}$ ;  $\text{CaBi}_2\text{Nb}_2\text{O}_9$

## 1. Introduction

Bismuth-layer structured ferroelectrics (BLSF) belongs to a large family of layered compounds with perovskite related structures, known as Aurivillius phases. Many compounds in this family exhibit a high Curie temperature ( $T_C$ ). They are lead-free, and have been proposed for high temperature piezoelectric and sensing applications.<sup>1,2</sup> The general formula of the Aurivillius phases is  $(\text{Bi}_2\text{O}_2)^{2+}(\text{A}_{m-1}\text{B}_m\text{O}_{3m+1})^{2-}$ , where A is a mono-, di- or trivalent element (or a combination of them) with cub-octahedral coordination; B is an octahedral coordinated transition metal; and  $m$  represent the number of octahedral layers in the perovskite slab.  $\text{Bi}_4\text{Ti}_3\text{O}_{12}$  exhibit a monoclinic symmetry with  $m = 3$  while the symmetry of  $\text{CaBi}_2\text{Nb}_2\text{O}_9$  is orthorhombic with  $m = 2$ .

Due to the layered structure features, the single crystals of Aurivillius phases exhibit highly anisotropic properties.<sup>3,4</sup> Polycrystalline ceramic materials based on them exhibit, however, often isotropic physical properties as the grains usually are randomly oriented. In order to improve the physical properties textured, e.g. grain-oriented, microstructures of Bi-layer structured ferroelectric ceramics have been produced via: (i) preparation of powders with needle/platelet morphology and aligning them via a shear flow process and allowing them to grow into aligned grains, via the Ostwald ripening mechanism, by heat treatment at elevated temperatures<sup>5,6</sup>; (ii) In order to improve the grain alignment even further a small part of well-developed large (2–5  $\mu\text{m}$ ) needles/platelets are added as grain growth templates.<sup>7,8</sup> An increase of the initial size of the templates promotes increasing the degree of grain alignment, however, slows down both the densification rate and the grain alignment, implying an unfavourable prolongation of the processing time.

In a recent article we outlined a new processing concept to produce highly textured compacts of  $\text{Bi}_4\text{Ti}_3\text{O}_{12}$  and made an

\* Corresponding author. Tel.: +46 8 162388; fax: +46 8 152187.  
E-mail address: [shen@inorg.su.se](mailto:shen@inorg.su.se) (Z. Shen).

extended evaluation of properties, mainly the dielectric ones, of the textured samples.<sup>9</sup> Here we present a more detailed study on this topic: (i) studies of the sintering behaviour of nano-sized  $\text{Bi}_4\text{Ti}_3\text{O}_{12}$  and micron-sized  $\text{CaBi}_2\text{Nb}_2\text{O}_9$  powders; (ii) preparation of appropriate pre-forms by spark plasma sintering (SPS) and subject them for superplastic deformation in the SPS unit; (iii) studies of the evolution of the microstructure of obtained compacts as function of the sintering and deformation conditions applied; (iv) a discussion of the obtained data with reference to the underlying mechanisms that yield highly textured ceramics.

## 2. Experimental procedure

### 2.1. Starting powders

The nano-sized  $\text{Bi}_4\text{Ti}_3\text{O}_{12}$  (abbreviated BIT below) powder was prepared from  $\text{Bi}(\text{NO}_3)_3 \cdot 5\text{H}_2\text{O}$  and  $\text{Ti}(\text{OC}_4\text{H}_9)_4$  using a hydrolysis technique. The resulting product was heat treated at  $600^\circ\text{C}$  for half an hour yielding a monophasic well-crystallized  $\text{Bi}_4\text{Ti}_3\text{O}_{12}$  powder with a BET surface area of  $12\text{ m}^2\text{ g}^{-1}$  and an average particle size of  $100\text{ nm}$ .<sup>10</sup> Subsequent X-ray and SEM/TEM studies did not reveal the presence of any secondary phases.

The  $\text{CaBi}_2\text{Nb}_2\text{O}_9$  (CBNO) powders were obtained by calcination of appropriate amounts of  $\text{Bi}_2\text{O}_3$  (ALFA, 99.975%),  $\text{CaCO}_3$  (ALDRICH, 99%) and  $\text{Nb}_2\text{O}_5$  (ALFA 99.9%) at  $950^\circ\text{C}$  for 4 h as described by Yan et al. The grain size of the resulting powder was in the range of  $0.7\text{--}1\text{ }\mu\text{m}$ .<sup>11</sup>

### 2.2. Sintering and superplastic deformation

The precursor powders were compacted in vacuum in a spark plasma sintering (SPS) apparatus, Dr. Sinter 2050 (Sumitomo Coal Mining Co. Ltd., Japan). The precursors powders were loaded in cylindrical graphite dies with an inner diameter of  $12\text{ mm}$  and heated to the final sintering temperature using a heating rate of  $100^\circ\text{C min}^{-1}$  and a uniaxial pressure of  $50\text{ MPa}$ . Pressures of  $75$  or  $100\text{ MPa}$  were used at the lowest sintering temperatures in order to ensure full densification. In the temperature range  $T < 1000^\circ\text{C}$  the temperature was measured and regulated by a thermal couple, that was inserted into the die while for  $T \geq 1000^\circ\text{C}$  the temperature was measured and regulated by an optical pyrometer focused on the surface of the die. The linear shrinkage and shrinkage rate discussed below are defined as  $-\Delta L/L_0$  and  $d(-\Delta L/L_0)/dt$ , respectively, with  $L_0$  being the thickness of the sample at room temperature with pressure applied. The  $\Delta L$ -values were corrected for the contribution of thermal expansion of the die. Since the mass and diameter of the sample are constant during SPS processing, the linear shrinkage defined above also represents the volume shrinkage, and can thus be converted to density values. Fully dense cylindrical compacts with a diameter of  $12\text{ mm}$  and a height of  $5\text{--}7\text{ mm}$  of BIT were prepared at  $800^\circ\text{C}$  using a pressure of  $75\text{ MPa}$  and a holding time of  $5\text{ min}$ , and these compacts contained equi-axed nano-sized BIT grains and corresponding CBNO compacts (containing micron-sized grains) were prepared at  $925^\circ\text{C}$  using a pressure of  $100\text{ MPa}$  and a holding time of  $3\text{ min}$ . These

compacts were placed in a pressure die with inner diameter of  $20\text{ mm}$ , and the BIT and CBNO compacts were heated in vacuum to  $1000$  and  $1150^\circ\text{C}$ , respectively, using a heating rate of  $100^\circ\text{C min}^{-1}$ . A constant uniaxial load that corresponded to an initial compressive stress of  $40\text{ MPa}$  was applied at room temperature or at the preset temperature. The compressive deformation strain is defined as  $-\Delta L_d/L_0$ , where  $\Delta L_d$  and  $L_0$  represent the shrinkage of sample height and the original height of the sample before deformation, respectively. Both of the  $\Delta L_d$  and  $L_0$  values were corrected for the contribution related to the expansion of the die. The strain rate is defined as  $d(-\Delta L_d/L_0)/dt$ .

### 2.3. Characterization

The densities were measured according to Archimedes' principle. The microstructures of the prepared samples were recorded in scanning electron microscopes (JEOL 880 and JSM 6300). Thermal etched surfaces were depicted and the grain size was determined by using an image analysis program (Image tool, UTHSCSA) through investigating more than  $100$  grains. The X-ray diffraction patterns were recorded both in a Guinier–Hägg camera and a STOE diffractometer. The Lotgering orientation factor  $f = ((p - p_0)/(1 - p_0))$  with  $p = (\sum I_{001} / \sum I_{hkl})$  and  $p_0$  for a random orientation powder pattern was calculated using intensities for  $120$  reflections at  $2\theta \leq 69^\circ$ . The preferred orientation was in the refinement modelled by the March–(Dollase) function,<sup>12</sup>

$$O_{\text{ph}} = \left( R_0^2 \cos^2 A + \frac{\sin^2 A}{R_0} \right)^{-3/2}$$

where  $A$  is the angle between the preferred orientation axis  $(001)$  and the reflection vector.

## 3. Results

### 3.1. Sintering behaviour of $\text{Bi}_4\text{Ti}_3\text{O}_{12}$ and $\text{CaBi}_2\text{Nb}_2\text{O}_9$

The sintering behaviour of the  $\text{Bi}_4\text{Ti}_3\text{O}_{12}$  (BIT) and  $\text{CaBi}_2\text{Nb}_2\text{O}_9$  (CBNO) samples has been investigated using a heating rate of  $100^\circ\text{C min}^{-1}$  and a pressure of  $50\text{ MPa}$ . The normalized shrinkage of the samples is plotted versus the temperature in Fig. 1. The densification process of both powders progresses very rapidly, i.e. the densification occurs within a very narrow temperature interval ranging from  $\sim 650$  to  $\sim 850^\circ\text{C}$  for the BIT powder and from  $\sim 825$  to  $\sim 1000^\circ\text{C}$  for the CBNO powder. The nano-sized powder of BIT shows a lower densification onset temperature ( $\sim 650^\circ\text{C}$ ) and higher maximum shrinkage rate,  $8.9 \times 10^{-3}\text{ s}^{-1}$  at  $780^\circ\text{C}$ , than the micron-sized powder of CBNO ( $\sim 825^\circ\text{C}$  and  $4.5 \times 10^{-3}\text{ s}^{-1}$  at  $950^\circ\text{C}$ , respectively).

The nano-sized BIT powder has been isothermally densified in temperature interval of  $750\text{--}1000^\circ\text{C}$ . Densities larger than  $97\%$  of theoretical value (TD) were achieved for samples prepared in the temperature region from  $775$  to  $850^\circ\text{C}$  by using a pressure of  $75\text{ MPa}$  and applying a holding time of  $3\text{ min}$ ,

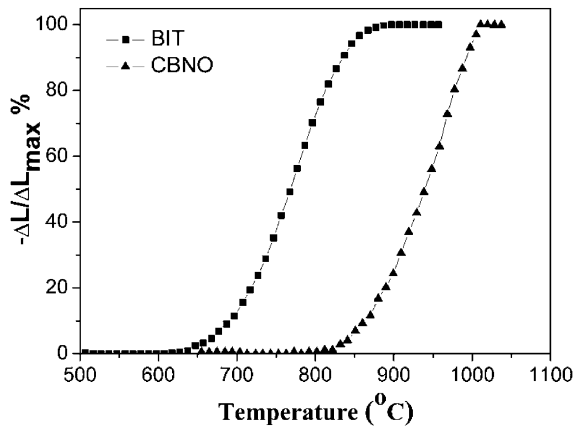


Fig. 1. Normalized shrinkage plotted vs. the temperature for  $\text{Bi}_4\text{Ti}_3\text{O}_{12}$  (BIT) and  $\text{CaBi}_2\text{Nb}_2\text{O}_9$  (CBNO) using a heating rate of  $100\text{ }^{\circ}\text{C min}^{-1}$  and a pressure of 50 MPa.

while for samples prepared at  $T > 850\text{ }^{\circ}\text{C}$  a pressure of 50 MPa and no holding time was used. The microstructures of samples compacted at different temperatures are shown in Fig. 2. The obtained grain sizes and density data at the various densification temperatures,  $T_{\text{iso}}$ , plotted versus  $T_{\text{iso}}$  in Fig. 3 and a “kinetic window” is revealed within which full densification is achieved paired with a very limited grain growth. The kinetic window is as broad as  $75\text{ }^{\circ}\text{C}$  ranging from 775 to  $850\text{ }^{\circ}\text{C}$  while elongated grains are very rapidly formed at the temperatures exceeding  $850\text{ }^{\circ}\text{C}$ , thus constitutes the onset temperature ( $T_g$ ) of grain growth. Equi-axed grains of the size  $150\text{ nm}$  are thus found in samples prepared at  $800\text{ }^{\circ}\text{C}$  (see Fig. 2a) while at  $1000\text{ }^{\circ}\text{C}$  grains with an average length of  $2.6\text{ }\mu\text{m}$  along  $ab$  direction and with an average width and thickness of  $0.52\text{ }\mu\text{m}$  is formed (see

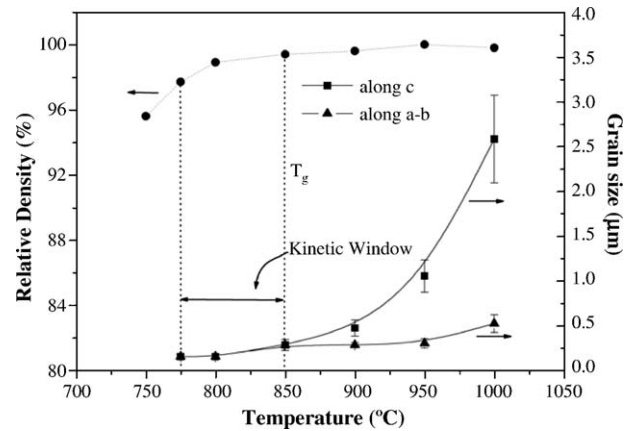


Fig. 3. Relative densities and grain sizes of BIT samples plotted vs. sintering temperature. The kinetic windows within which fully dense nano-sized ceramics were obtained are marked. Above  $T_g$ , the grains elongated platelet grains were rapidly formed. The grain growth along  $ab$  direction is much faster than that along  $c$  direction.

Fig. 2d). The length and width (thickness) of the grains increase with increasing sintering temperature as seen in Fig. 2.

CBNO compacts with densities of 95% TD or more can be prepared at  $T \geq 925\text{ }^{\circ}\text{C}$  using a pressure of 100 MPa and 3 min holding time. The microstructure of the CBNO compact prepared  $925\text{ }^{\circ}\text{C}$  reveals the presence of small platelet grains as the starting powder. SEM studies of samples prepared above  $925\text{ }^{\circ}\text{C}$  revealed that these compacts consisted mostly of large grains with substantial smaller length to width ratios comparing with those observed in the BIT compacts, i.e. of similar size and form as those depicted in Fig. 7.

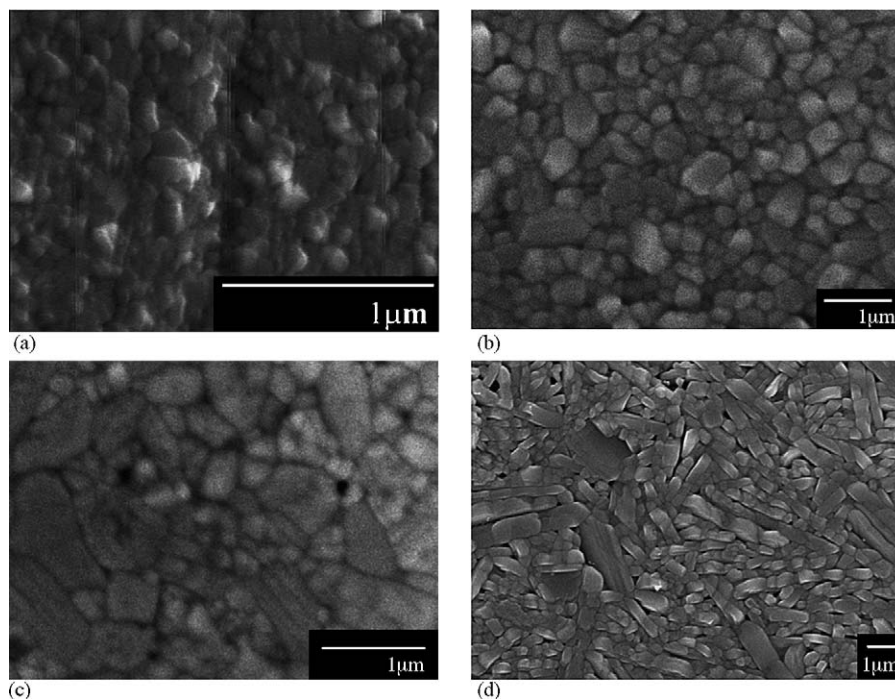


Fig. 2. SEM micrographs of BIT samples sintered at: (a)  $800\text{ }^{\circ}\text{C}$ , (b)  $850\text{ }^{\circ}\text{C}$ , (c)  $950\text{ }^{\circ}\text{C}$ , and (d)  $1000\text{ }^{\circ}\text{C}$ . A uniaxial pressure of 50 MPa and no holding time was used for samples prepared at  $T > 850\text{ }^{\circ}\text{C}$ , while for the samples prepared at  $T \leq 850\text{ }^{\circ}\text{C}$  a pressure of 75 MPa, a holding time of 3 min was used.

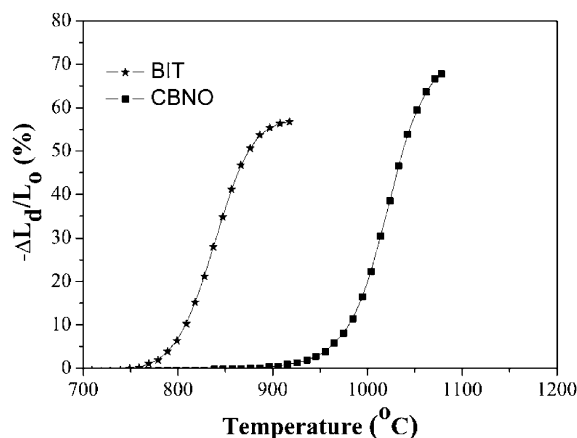


Fig. 4. Normalized compressive deformation strain of the BIT and CBNO samples plotted vs. temperature. A heating rate of  $100\text{ }^{\circ}\text{C min}^{-1}$  and a constant load corresponding to an initial compressive stress of 40 MPa was used.

### 3.2. Superplastic deformation yielding textured microstructures

Fig. 4 reveals the compressive deformation strains plotted versus temperature. The deformation process of BIT sample started at  $\sim 760\text{ }^{\circ}\text{C}$ , while that of the CBNO sample is activated at  $\sim 920\text{ }^{\circ}\text{C}$ . The recorded maximum compressive strain rate is  $1.1 \times 10^{-2}\text{ s}^{-1}$  at  $\sim 840\text{ }^{\circ}\text{C}$ , and  $1.3 \times 10^{-2}\text{ s}^{-1}$  at  $1020\text{ }^{\circ}\text{C}$  for BIT and CBNO, respectively.

The deformation compressive strain and strain rate of BIT samples isothermally recorded at different temperatures are plotted versus time in Fig. 5. In these cases the pressure is applied when the preset temperature is reached. It is evident that both the compressive strain and strain rate increased with increasing deformation temperature.

Isothermal deformation experiments of a series of BIT samples with different microstructures, i.e. exhibiting the nano-sized, sub-micron-sized and micron-sized structures depicted in Fig. 2a, b, and c, have also been performed. The deformation experiments were carried out at  $850\text{ }^{\circ}\text{C}$ , and as above the pressure is applied when the preset temperature is reached. The recorded strain data are plotted versus time in Fig. 6. The deformation strain of the nano-sized sample is obviously higher than the sub-micron-sized one and substantial higher than the micron-sized one.

### 3.3. SEM and X-ray diffraction studies

Scanning electron micrographs of the samples after superplastic deformation, viewed parallel and perpendicular to the shear flow direction are shown in Fig. 7. It is clearly shown that: (i) in the BIT samples the formed grains are thin, well faceted, elongated and fairly randomly orientated parallel to the shear flow direction, whereas they pile up themselves in the perpendicular direction, yielding compacts with 2D microstructures; and (ii) in the CBNO sample the degree of grain alignment is less pronounced.

X-ray diffraction patterns of the surfaces of BIT and CBNO samples parallel to the shear flow direction are shown in Fig. 8

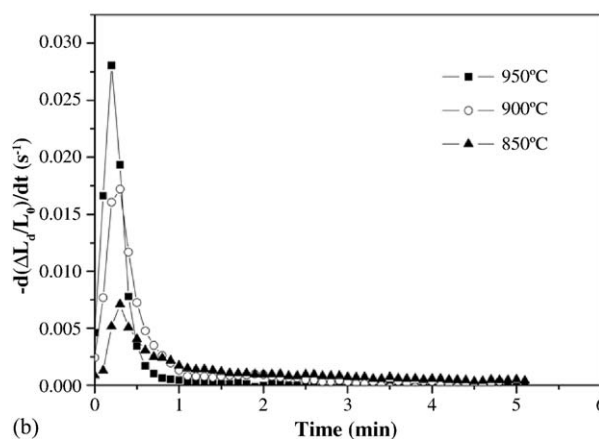
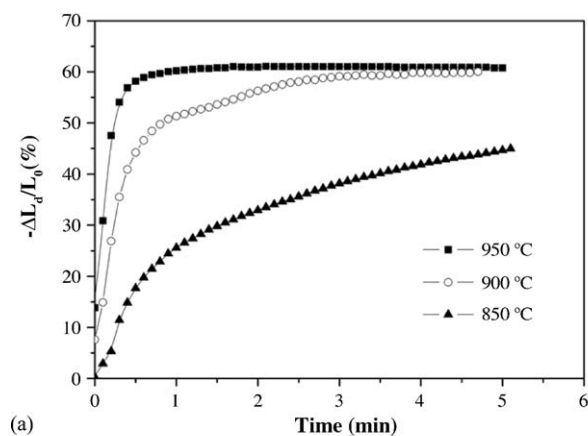


Fig. 5. Normalized compressive deformation strain (a) and deformation strain rate (b) of the BIT sample deformed at different temperatures plotted vs. time. A load corresponding to an initial compressive stress of 40 MPa was used at the preset temperature.

and no reflections foreign to the parent compounds are found. The XRD patterns exhibited strong (001) diffraction peaks verifying the highly textured feature of the samples. A Lotgering orientation factor of 99% was recorded for the textured BIT sample while the one for the CBNO sample was 70%.

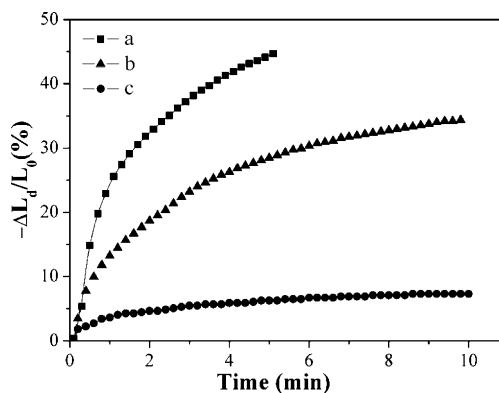


Fig. 6. The deformation strains of the series BIT samples with (a) nano-sized, (b) sub-micron-sized, and (c) micron-sized structures deformed at  $850\text{ }^{\circ}\text{C}$  plotted vs. time. A load corresponding to an initial compressive stress of 40 MPa was used.



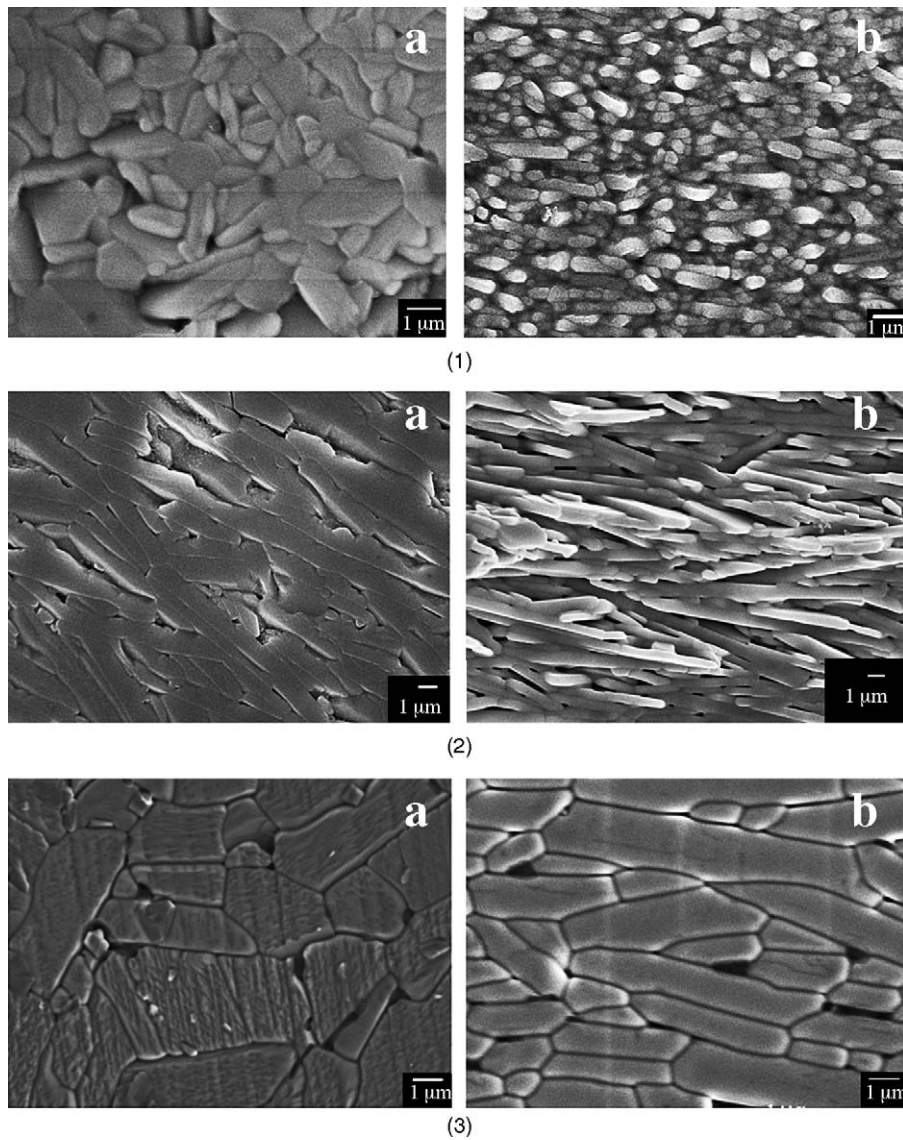


Fig. 7. SEM micrographs taken on the polished and thermally etched surfaces of BIT samples deformed at 900 °C (holding time 5 min) (1), at 1000 °C (10 min) (2), and CBNO sample deformed at 1150 °C (5 min) (3), parallel (a) and perpendicular (b) to the shear flow direction.

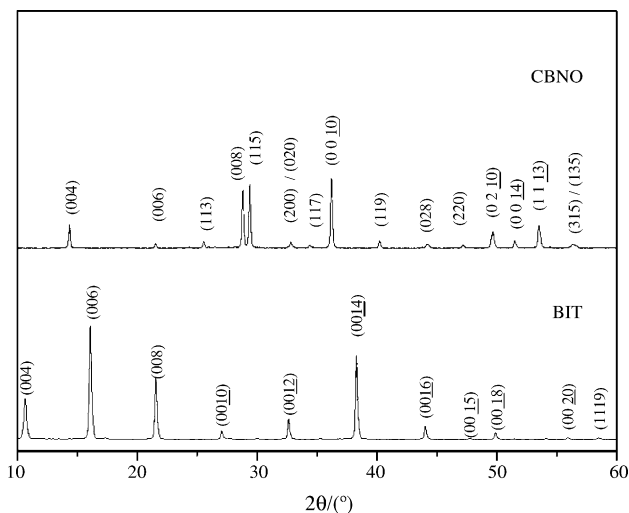


Fig. 8. X-ray diffraction (XRD) patterns of the surfaces oriented parallel to the shear flow direction.

#### 4. Discussion

We have shown above that it is possible to fully consolidate nano-sized BIT powder within the temperature region  $750^{\circ}\text{C} < T < 850^{\circ}\text{C}$  thus to obtain compacts consisting of grains with similar size as the precursor powder. At temperatures exceeding  $850^{\circ}\text{C}$  the compacts contained elongated randomly oriented grains and the aspect ratio increases with increasing temperature. In fact, the transformation from equi-axed grains to elongated platelet grains with a high aspect ratio goes very fast, i.e. at  $800^{\circ}\text{C}$  the compacts contain equi-axed nano-sized grains while at  $1000^{\circ}\text{C}$ , 2 min later as we used a heating rate of  $100^{\circ}\text{C}$ , the compacts contained elongated platelet grains with the  $a$ -axis  $\gg b$ -axis  $>$  or  $\cong c$ -axis. The micron-sized CBNO powder could be compacted with limited grain growth at  $925^{\circ}\text{C}$  while at higher temperatures ( $1000^{\circ}\text{C}$ ) platelet grains with low aspect ratio are formed implying that the possibilities to tailor the microstructures is

much more restricted when micron-sized precursor powder is used.

The main features of the isothermal deformation experiments suggested that: (i) the deformation of compacts consisting of equi-axed nano-sized grains proceeds very fast, i.e. compressive strain rates of the order  $10^{-2} \text{ s}^{-1}$  can easily be achieved. The deformation of compacts containing sub-micron-sized equi-axed grains proceeds less fast, and that of containing randomly oriented elongated platelet grains is very much retarded; (ii) above a critical temperature the conversion of nano- to micron-sized grains progresses very rapidly, where the superplastic deformation is associated with a transportation of the randomly oriented nano-sized grains into an almost 100% aligned elongated platelet grains with aspect ratios exceeding 10; (iii) the aspect ratio of the grains in deformed samples can be tailored by mastering the deformation temperature and time.

It is well known that the elongated growth takes place along the *ab* direction of the unit cell of the BIT phase. It is commonly assumed that this is due to anisotropic interfacial energies. We have previously observed that rapid anisotropic grain growth also can occur in  $\text{Si}_3\text{N}_4$ -based systems when high heating rates are applied via a dynamic ripening mechanism.<sup>13</sup> In the latter case a liquid is present that facilitate the transportation of appropriate species from one place to another. X-ray and SEM-EDS studies of polished but not etched surfaces of compacted and deformed BIT samples have not revealed the presence of any secondary phase, i.e. a phase such as  $\text{Bi}_2\text{O}_3$  or  $\text{Bi}_{12}\text{TiO}_{20}$  with melting points below or in the vicinity of the compaction and deformation temperatures, which would provide the system with a liquid phase at temperatures exceeding  $\sim 825^\circ\text{C}$  that in turn would facilitate the deformation and compaction processes. As no liquid seems to be present a very fast grain boundary diffusion process ought to be present. The use of fast heating rates seems to be essential, i.e. when a nano-sized BIT sample is very fast brought up to a temperature that substantially exceeds the onset temperature of grain growth ( $\sim 850^\circ\text{C}$ ) the driving force for grain growth becomes large and the most efficient way for the system to respond to this force is to preferentially localize appropriate species onto the crystallographic surfaces that will most easily accommodate them yielding a microstructure that contain elongated and randomly oriented grains. The driving force for grain growth should accordingly decrease with increasing grain size of the precursor powder in agreement with our experimental findings, i.e. CBNO compacts containing elongated and randomly oriented grains could hardly be produced due to the use of a micron-sized precursor powder.

When a fully dense nano-sized BIT compact is exposed to compressive strain at  $T > T_g$  the driving force for grain growth seems to be even larger. In this case the grain growth preferentially takes place parallel to the shear flow direction and an almost perfect grain-aligned compact consisting of elongated platelet grains with the *a*-axis  $\gg$  the *b*-axis or  $\cong$  the *c*-axis is formed within minutes, i.e. the superplastic deformation process induced a directional dynamic ripening process that in turn yielded a highly grain-aligned, textured, compact. The density of

the deformed compact is very similar to that of the pre-compact implying that the deformation does not induce formation of pores in spite of that amount of material that is transported from one place to another is large at a strain of  $\sim 60\%$ . The resulting microstructure of deformed compact is strongly dependent on the microstructure of the pre-densified compact to be deformed as illustrated by the observation that: (i) a pre-densified compact consisting of randomly oriented elongated platelet grains is very difficult to deform; (ii) the compressive deformation experiments using micron-sized pre-densified compacts of the CBNO composition yield compacts that are substantial less well grain-aligned compacts and the degree of alignments obtained is in fact of similar size as that obtained by the grain alignment processes discussed above.

## 5. Concluding remarks

We have shown above that using a nano-sized starting BIT powder we can prepare fully dense BIT compacts that contain grains of similar size as the starting powder. This implies that the compaction mainly occurs via grain sliding along grain-boundaries. In the past, numerous works have aimed to improve superplasticity of ceramics by diminishing the sliding resistance via doping and reducing the grain size. In all these studies the grain sliding process was activated thermally, i.e. by applying a high enough temperature. Such a thermal activated grain sliding process relies on the grain boundary diffusion that in turn also is responsible for the grain growth. Accordingly, one has observed in connection with compressive deformation of ceramics grain growth that the deformation process proceeds fairly fast during the initial part of the deformation but is soon retarded by grain growth induced strain hardening. Our studies show that utilising the SPS technique, i.e. performing the compaction and deformation experiments in presence of a pulsed electrical field that in turn promote mass transport, the kinetic window that separates the grain sliding mechanism from the grain growth one is enlarged. Through exploiting the difference in kinetics between grain growth and grain sliding and by selectively activating the grain sliding process we have observed that compressive strains rates in the range of  $10^{-2} \text{ s}^{-1}$  can be achieved.

The rapid grain growth that occurs in an unpredictable manner is usually regarded as abnormal grain growth. However, if it can be used in a controlled manner, grain-aligned microstructures such as those described above can be obtained. Our findings suggest that the grain growth rate is radically enhanced by the reduction of the initial grain size, and it is quite predicable that rapid grain growth will occur if one is able to bring the initial fine particles/grains to high temperatures via the use of rapid heating rates. The rapid grain growth will be even further enhanced when additional driving forces that promotes mass transport is brought in, i.e. when the deformation takes place under pressure and in presence of a pulsed electrical field. The mechanism behind such a rapid grain growth and grain alignment process has been termed by us as a superplastic deformation-induced directional dynamic ripening.

## Acknowledgement

The work was supported by the Swedish Research Council through grant 621-2002-4299 and the National Natural Science Foundation of China through grants 50328203 and 50472013.

## References

1. Damjanovic, D., Materials for high-temperature piezoelectric transducers. *Curr. Opin. Solid State Mater. Sci.*, 1998, **3**, 469–473.
2. Park, B. H., Kang, B. S., Bu, S. D., Noh, T. W., Lee, J. and Jo, W., Lanthanum-substituted bismuth titanate for use in non-volatile memories. *Nature (London)*, 1999, **401**, 682–684.
3. Sakata, K., Takenaka, T. and Shoji, K., Hot-forged ferroelectric ceramics of some bismuth compounds with layer structure. *Ferroelectrics*, 1978, **22**, 825–826.
4. Takenaka, T., Nagata, H. and Suzuki, M., Bismuth layer-structured ferroelectrics with high curie temperatures. *Ceram. Int.*, 2004, **30**, 2053.
5. Holmes, M., Newnham, R. E. and Cross, L. E., Grain-oriented ferroelectric ceramics. *Am. Ceramic Soc. Bull.*, 1979, **58**, 872.
6. Kimura, T., Yoshimoto, T., Iida, N., Fujita, Y. and Yamaguchi, T., Mechanism of grain orientation during hot-pressing of bismuth titanate. *J. Am. Ceram. Soc.*, 1989, **72**, 85–89.
7. Horn, J. A., Zhang, S. C., Selvaraj, U., Messing, G. L. and Trolier-McKinstry, S., Templated grain growth of textured bismuth titanate. *J. Am. Ceram. Soc.*, 1999, **82**, 921–926.
8. Watanabe, H., Kimura, T. and Yamaguchi, T., Particle orientation during tape casting in the fabrication of grain-oriented bismuth titanate. *J. Am. Ceram. Soc.*, 1989, **72**, 289–293.
9. Shen, Z., Liu, J., Grins, J. et al., Effective grain alignment in ceramics by superplastic deformation induced directional dynamic ripening. *Adv. Mater.*, 2005, **17**(6), 676–680.
10. Kan, Y., Wang, P., Li, Y., Cheng, Y. and Yan, D., Fabrication of textured bismuth titanate by templated grain growth using aqueous tape casting. *J. Eur. Ceramic Soc.*, 2003, **23**, 2163–2169.
11. Yan, H., Zhang, H., Ubic, R. et al., A lead free high curie point ferroelectric ceramic  $\text{CaBi}_2\text{Nb}_2\text{O}_9$ . *Adv. Mater.*, 2005, **17**, 1261–1265.
12. Dollase, W. A., Correction of intensities for preferred orientation in powder diffractometry: application of the March model. *J. Appl. Crystallogr.*, 1986, **19**, 267–272.
13. Shen, Z., Zhao, Z., Peng, H. and Nygren, M., Formation of tough interlocking microstructures in silicon nitride ceramics by dynamic ripening. *Nature (London, United Kingdom)*, 2002, **417**, 266–269.